Reactions of deuterated methanol (CD3OD) on Fe3O4(111)

ARTICLE *in* THE JOURNAL OF PHYSICAL CHEMISTRY C · JANUARY 2015

Impact Factor: 4.77 · DOI: 10.1021/jp510821g

THE JOURNAL OF PHYSICAL CHEMISTRY C

Article

pubs.acs.org/JPCC

Reactions of Deuterated Methanol (CD_3OD) on Fe_3O_4(111)

Zhisheng Li,[†] Denis V. Potapenko,[†] Kwang Taeg Rim,[‡,§] Maria Flytzani-Stephanopoulos,[∥] George W. Flynn,[‡,§] Richard M. Osgood,*[,†] Xiao-Dong Wen,[⊥,#,▽] and Enrique R. Batista[▽]

[†]Department of Applied Physics and Applied Mathematics, [‡]Department of Chemistry, and [§]Nanoscale Science and Engineering Center, Columbia University, New York, New York 10027, United States

[∥]Department of Chemical and Biological Engineering, Tufts University, Medford, Massachusetts 02155, United States

[⊥]State Key Laboratory of Coal Conversion, Institute of Coal Chemistry, Chinese Academy of Sciences, P.O. Box 165, Taiyuan, Shanxi 030001, People's Republic of China

[#]Synfuels China, Beijing 100195, People's Republic of China

[▽]Theoretical Division, Los Alamos National Laboratory, Los Alamos, New Mexico 87545, United States

ABSTRACT: We report an experimental and theoretical investigation of the decomposition (partial oxidation) of deuterated methanol (CD_3OD) on a single-crystal Fe_3O_4(111) surface. The crystal surface contains majority areas of a Fe-terminated Fe_3O_4(111) surface as well as smaller regions of O-terminated FeO(111) or biphase surface reconstruction. Our investigation uses a combination of scanning tunneling microscopy, temperature-programmed desorption, and density functional theory calculations to examine the surface reactions and adsorbates as a function of coverage. Our studies show that the reaction of methanol on this iron−oxide surface is highly sensitive to atomic-level surface reconstructions.

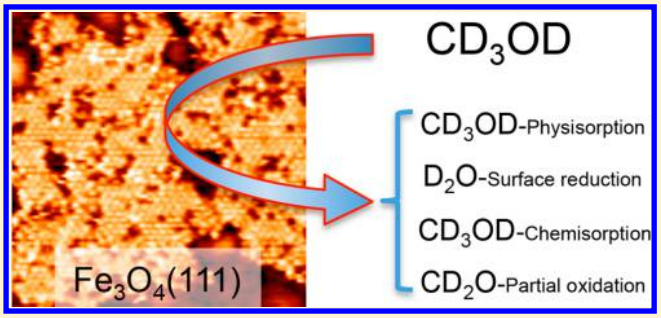

INTRODUCTION

The reaction of simple molecules with different iron oxide surfaces has been the subject of numerous studies, primarily due to the importance of iron oxide as a model mineral crystal for studying basic environmental processes but also due to its potential importance in hydrogen generation for fuel-cell applications.[1] Considering first the motivation for molecular-scale environmental research, there have been many recent studies of the decomposition of H_2O and other organic species such as CCl_4 on magnetite surfaces using scanning tunneling microscopy (STM), temperature-programmed desorption (TPD), and synchrotron X-ray photoelectron spectroscopy (SXPS).[2−9] One particularly important area of interest has been the variation of reactivity with the many surface reconstructions of magnetite. Despite the importance of reactions of common waste organic species that are mediated via iron−oxide surfaces, an investigation of alcohols with these same surfaces has been lacking.

The motivation for fuel-cell related studies of alcohols with iron oxides[10−14] is that alcohols have become very promising candidates as reforming substrates for on-demand H_2 production. In particular, the reactivity of the Fe_3O_4 (111) surface with methanol is of interest for fuel-cell technology applications because methanol is easy to store and transport, and can be derived from a variety of sources such as biomass.[15] There are three main processes by which methanol can be used to produce H_2: oxidative reforming (ORM), decomposition (DOM), and steam reforming (SRM)[16,17] of methanol; our experiments are focused on DOM. Thus, DOM has recently been investigated using model single-crystal iron−oxide surfaces in ultrahigh vacuum to further our understanding of the more complex heterogeneous reaction taking place on metal particles supported on reducible and irreducible oxide surfaces.[10]

In this article, we report the decomposition (partial oxidation) of fully deuterated methanol (CD_3OD) on a natural single-crystal Fe_3O_4(111) surface. The crystal is composed of majority areas of the Fe-terminated Fe_3O_4(111) surface as well as smaller regions consisting of O-terminated FeO(111) or the biphase surface reconstruction.[18−20] Our study employs scanning tunneling microscopy, temperature-programmed desorption, and density functional theory (DFT) calculations to investigate this catalytic surface reaction. The combination of TPD and STM imaging on the same surface allows us to relate specific reactivity patterns to different surface phases of Fe_3O_4(111). These phases could be easily distinguished from one another in the STM images. Our studies show that the reaction of methanol on an iron−oxide surface is highly sensitive to atomic-level surface reconstructions.

Received: October 28, 2014
Revised: December 22, 2014
Published: December 24, 2014

DOI: 10.1021/jp510821g
J. Phys. Chem. C 2015, 119, 1113−1120

EXPERIMENTAL AND THEORETICAL METHODS

The TPD experiments were conducted in a UHV chamber, which was equipped with a commercial Omicron VT-STM, an argon-ion sputtering gun, a LEED/Auger system, and a differentially pumped retractable VGQ mass spectrometer. The base pressure in the chamber was 8×10^{-11} Torr. A 5 × 5 mm $Fe_3O_4(111)$ sample was mechanically cut from a natural mineral crystal (purchased from SurfaceNet GmbH, Germany). The sample was attached to the surface of a Mo heating plate using Ta wires, and the plate was resistively heated via ceramic-potted nichrome wires. Direct temperature measurements were made using a K-type thermocouple, which was attached directly to the sample. Newly mounted samples were prepared in a UHV chamber by 20 cycles of sputtering with argon (1 keV, 10 min) and high-temperature annealing (1000 K) in oxygen (1×10^{-6} Torr). When cleaned according to this approach, the surface exhibited a sharp, ordered (2 × 2) LEED pattern. After initial preparation, one cleaning cycle was applied prior to reagent exposure. The cleanliness of the surface was checked by both LEED and STM imaging before dosing experiments were performed. Precise deuterated-methanol doses were administered through an aperture-based gas system, in which a gas line followed by a 5 μm aperture was filled with alcohol vapor in the mTorr pressure range for a desired amount of time. The other side of the aperture opened into a 4 mm-diameter tube leading toward the sample, which faced the UHV-side opening of this tube at a distance of approximately 5 mm. Before dosing, CD_3OD was purified by several freeze–pump–thaw cycles. After being cleaned, the $Fe_3O_4(111)$ sample was cooled by liquid nitrogen. The surface was then dosed with CD_3OD at ~134 K. This dosing was controlled by the preaperture pressure and dosing time. To obtain the TPD spectra, the 3 mm-diameter aperture on a conical exit tip of the mass spectrometer encasement was brought within ~1 mm of the sample's surface to reduce stray signals from the sample holder. Linear heating rates of 2 K/s, regulated by a PID-type temperature controller, were used in all TPD experiments.

Some STM images were collected in a second separate UHV chamber with a base pressure of 3×10^{-10} Torr. The chamber was equipped with an ion gun, rearview LEED optics (Princeton Research Instruments), a quadrupole mass spectrometer, and a commercial VT STM (Omicron GmbH) capable of scanning at temperatures ranging from 25 to 1500 K. The surface exhibited the same sharp, ordered LEED pattern after surface preparation as mentioned above, indicating the same level of surface cleanliness was obtained in these two chambers.

The theoretical simulation results in this article were based on plane wave expansions using the computational program VASP (Vienna Ab-initio Simulation Package).[21] The energy cutoff for the plane-wave basis was set to 500 eV. Scalar relativistic effects are included with the PAW–PBE potentials[22,23] available in the distributed code. The Brillouin zone was sampled by Monkhorst–Pack meshes of 9 × 9 × 1 for GGA+U (U_{eff} = 4.0 eV) calculations.[24] Convergence of the electronic degrees of freedom was met when the total (free) energy change and the band-structure energy change between two steps were both fractionally smaller than 1×10^{-5}. All structural parameters (atomic position, lattice constants) were relaxed using a conjugate-gradient algorithm until the Hellmann–Feynman forces were <0.01 eV/Å. To investigate reaction mechanisms on an iron–oxide surface with adsorbed alcohols, the climbing-image-nudged-elastic-band (CINEB) method was performed to search for transition states. The reaction path was discretized with eight intermediate images between the two minima connected by elastic springs, to prevent the images from sliding to the minima during the course of optimization. The corresponding activation energy for a reaction is set by the energy difference between the initial and transition state.

RESULTS AND DISCUSSION

Temperature-Programmed Desorption Experiments.

Organics. After a clean iron–oxide surface was prepared as described above, the sample was dosed with fully deuterated methanol and a set of temperature-programmed-desorption experiments was performed. Figure 1 shows a series of TPD spectra for seven specific deuterated-methanol-dosed surfaces, each with a starting temperature of 134 K. For any given CD_3OD exposure, the TPD spectrum was found to be repeatable for consecutive experiments, suggesting that the surface was not altered by exposure to CD_3OD during TPD experiments, for final ramping temperatures up to 1000 K.

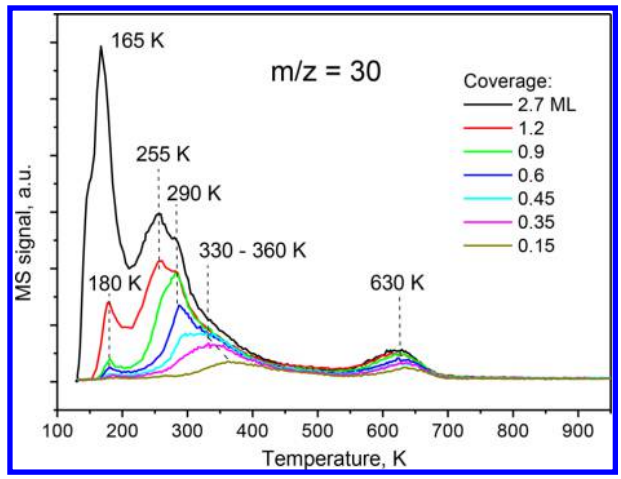

Figure 1. TPD spectra of molecular methanol on a $Fe_3O_4(111)$ surface, monitored at m/z = 30 (CDO^+), for seven dosing values.

The lowest-temperature desorption peak in these experiments is measured to be 165 K. This peak appears after a 0.6 ML dose (1 ML is defined as the onset coverage of multilayers), and then increases in amplitude as exposure increases, and remains unsaturated for exposures as high as 2.7 ML. We assign this peak to multilayer desorption, based on a comparison of our CD_3OD desorption peaks with those from other metal-oxides.[25,26] In addition, a small peak is measured at 180 K for coverages below 1 ML; this peak is attributed to physisorption at O-terminated areas as will be discussed in the section on STM measurements below.

Two strong TPD peaks are observed at 255 and 290 K. The 290 K peak first appears at an exposure of approximately 0.6 ML. With increasing coverage, it grows in intensity and saturates at 0.9 ML. At this same coverage, the 255 K desorption peak becomes noticeable. This second peak saturates at 1.2 ML methanol coverage. Importantly, both peaks stay at constant temperature positions with changing initial methanol coverage, which is characteristic of first-order desorption kinetics. A Redhead analysis of these two peaks reveals an approximate binding energy of 0.69 and 0.79 eV

DOI: 10.1021/jp510821g
J. Phys. Chem. C 2015, 119, 1113–1120

corresponding to the 255 and 290 K TPD peaks, respectively. These desorption energies are comparable to those expected for physisorbed species (see, for example, physisorbed methanol on $TiO_2(110)$[25]) and are of comparable magnitude to the DFT calculated value (−0.84 eV) for molecular-methanol adsorption at Fe sites of $Fe_3O_4(111)$ domains. We thus assign both of these peaks to molecular desorption from different Fe-terminated domains of the sample surface. The presence of two peaks and the small discrepancy between the DFT-calculated and experimentally observed binding energies will be addressed in the following sections.

In addition, two additional TPD peaks, one at 360 K and one at 630 K, are observed at low exposure (e.g., 0.15 ML) of this surface to CD_3OD, as shown in the data of Figure 1. Both peaks increase in intensity with increasing exposure, but the peak at 360 K progressively shifts toward a value of 330 K as exposure increases. This shift of the 360 K peak is characteristic of second-order desorption. We assign this peak to recombinative desorption of CD_3OD, an assignment supported by our STM experiments and DFT calculations. This recombinative desorption follows molecular methanol (CD_3OD) dissociative adsorption (eq 1) on $Fe_3O_4(111)$ with a calculated adsorption energy of −1.38 eV (see DFT section). Our assignments are also supported by observations of the dissociation of methanol into a methoxy radical bound to metal ions, and a hydrogen atom bound to lattice oxygen ions on oxide surfaces such as MgO[26] and $TiO_2(110)$.[25] We will also argue below that this recombination reaction most likely involves methoxy and D as denoted in eq 2; again this assignment is attributed to observations of comparable behavior on other oxides such as $TiO_2(110)$.[25]

$$CD_3OD_{gas} \rightarrow CD_3O_{ads} + D_{ads} \quad (1)$$

$$CD_3O_{ads} + D_{ads} \rightarrow CD_3OD_{gas} \quad (2)$$

To consider the highest-temperature desorption peak at 630 K, a sample spectrum at a coverage of 0.35 ML and at higher magnification is shown in Figure 2. Our mass spectroscopy indicates that this peak involves further surface reactions. To identify this peak, we use the fact that the mass spectroscopy ion-signal ratios for this 630 K peak are distinctly different (see Figure 2) from the lower-temperature peaks. In particular, for example, for all of the TPD peaks below 500 K, the signal ratios for ion masses m/z = 30, 32, 34, and 36 remain nearly constant for all experiments, indicating that the only CO-containing desorption product was methanol CD_3OD. However, m/z = 32 has the lowest signal among the four mentioned ion masses of the 330 K peak but is the second highest signal for the peak at 630 K. More detailed analysis shows that if we take m/z = 34 as a reference signal, representing fully deuterated methanol, and subtract methanol contributions from the other three signals, only m/z = 30 and 32 signals, with approximate 1:1 ratios, remain in the 630 K peak. These signals indicate the presence of an additional product other than methanol, in the 630 K TPD peak. In fact, the ion fragmentation pattern closely resembles the published fragmentation pattern of formaldehyde CD_2O.[27] Thus, we interpret our TPD data as simultaneous desorption of CD_3OD and CD_2O at around 630 K. This attribution is also supported by measurements on other oxide surfaces. In particular, methanol has been shown to partially oxidize to formaldehyde on a CeO_2-supported vanadium oxide surface. Depending on the vanadium oxidation state, the formaldehyde desorption peak appeared from 525 to 610 K, a value close to that of 630 K in our experiments.[28]

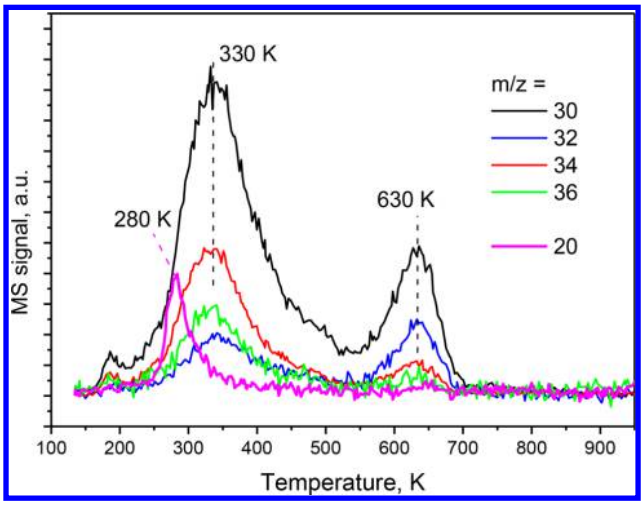

Figure 2. TPD spectrum with 0.35 ML methanol coverage showing different values of m/z. The changing ratio between m/z = 30, 32, 34, and 36 signals indicates the presence of formaldehyde CD_2O in the 630 K peak. A water desorption peak (m/z = 20) is observed at 280 K, which coincides with the rising edge of the methanol desorption peak.

At a more detailed level, our TPD measurements suggest that as the surface temperature increases, methoxy (CD_3O) attached to Fe^{III} sites is further dissociated into formaldehyde (CD_2O) and D atoms via C−D bond scission. Because of its weak surface bond (see Figure 5), formaldehyde formed from methoxy dissociation at high temperature can be expected to desorb immediately from the surface. The D atoms formed from the dissociation of methoxy can, in turn, recombine with excess, unreacted methoxy to desorb as methanol (CD_3OD) because this desorption channel is activated already at 360 K (see eq 2). The proposed surface reaction mechanism at high temperature can be written as follows:

$$CD_3O_{ads} \rightarrow CD_2O_{ads} + D_{ads} \quad (3)$$

$$CD_2O_{ads} \rightarrow CD_2O_{gas} \quad (4)$$

$$CD_3O_{ads} + D_{ads} \rightarrow CD_3OD_{gas} \quad (5)$$

In this set, eq 3 is the rate-limiting step for the group of processes that would account for the observed first-order desorption kinetics. The surface reactions described by eqs 3, 4, and 5 can be summarized as a disproportionation reaction shown in eq 6:

$$2CD_3O_{ads} \rightarrow CD_3OD_{gas} + CD_2O_{gas} \quad (6)$$

Water. In addition to the organic species discussed above, we have also observed a D_2O desorption peak in our TPD spectra over the 220−330 K temperature range. In particular, Figure 2 shows thermal desorption traces for 0.35 ML of CD_3OD on a $Fe_3O_4(111)$ surface. The m/z = 30, 32, 34, and 36 traces are fragmentation products from methanol and formaldehyde, as explained earlier. However, the shape of the m/z = 20 trace is not replicated by any of these four higher mass signals and thus did not originate from ionization processes in the mass spectrometer but rather must be a product of surface reactions. By analysis of the concurrent detected m/z = 18 and 17 signals, we conclude that the m/z = 20 trace originates from desorption of water D_2O. Separate

DOI: 10.1021/jp510821g
J. Phys. Chem. C 2015, 119, 1113−1120

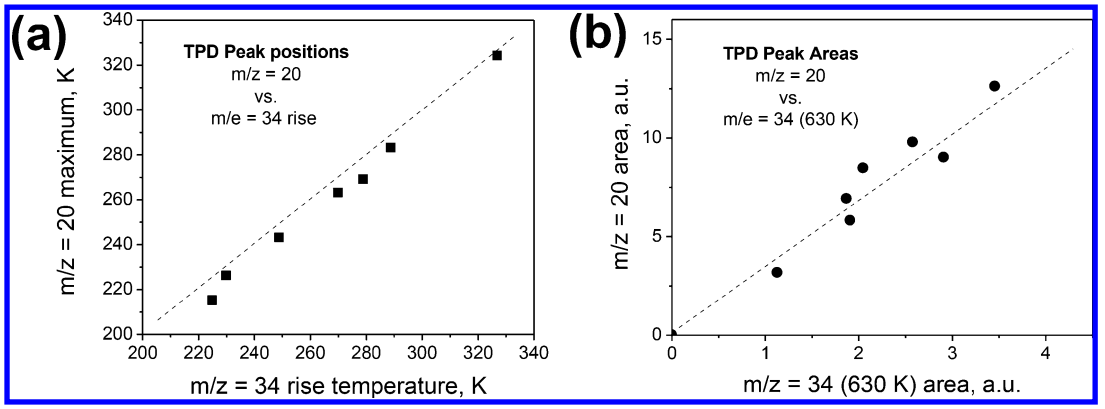

Figure 3. (a) Comparison of the water desorption peak temperature with the position of the rising edge of methanol desorption (i.e., the temperature of the maximum slope) for the seven TPD experiments shown in Figure 1. The dashed line marks the $y = x$ line. (b) Comparison of the TPD peak areas of water desorption at 220−320 K monitored at $m/z = 20$ and the methanol desorption at 630 K monitored at $m/z = 34$. The dashed line is a linear fit to the data.

TPD experiments with a Au(111) sample, which are not shown here, were used to show conclusively that neither our methanol source nor residual gases in the chamber deposited any detectible water on the surface during methanol dosing.

To establish the origin of the D_2O water desorption, we consider two observations that follow from our TPD data. First, the temperature of the D_2O desorption peak coincided with the rising edge of methanol desorption in the 200−400 K range. This relation can be seen for the 0.35 ML coverage experiment in Figure 2 and is summarized for all coverages in Figure 3a. Such a dependence implies a common desorption mechanism for water and methanol over this temperature range. The interrelation between water desorption and the low-temperature methanol desorption, presented in Figure 3a, involves competing reactions because at low coverages (0.15 and 0.35 ML) the rising edge of methanol desorption corresponds to the recombination reaction, eq 2, while at higher coverages this edge corresponds to molecular desorption. Our data allow only a tentative explanation for this observation. In particular, we propose that D_2O_{ads} molecules form from D_{ads} as a result of methanol chemisorption and extraction of some weakly bound O atoms on the $Fe_3O_4(111)$ surface at temperatures below 220 K (perhaps during deposition). Thus, the sample surface is partially reduced after each TPD run, and this change is expected to cause variations in the TPD spectrum in following experiments. Surprisingly, such a change is not observed in our TPD experiments; rather, the consecutive TPD spectra were very consistent. This absence of change suggests that the surface reduction is compensated by oxygen diffusing out from the bulk during high temperature annealing (1000 K, the end temperature of each TPD experiment). Therefore, the surface structure is recovered after each TPD experiment, making reduction of the sample unobservable with either TPD or STM. A similar reaction channel of extracting surface oxygen was also observed for CCl_4 adsorbed at this surface.[5] In particular, it was shown that CCl_4 dissociated into CCl_2 upon adsorption and desorbed as $OCCl_2$ with removal of surface oxygen. The onset of this desorption was ∼250 K, which falls into the same temperature range as our observations.

The second observation derived from our TPD experiments using different methanol exposures is that the total area of the TPD peak from water desorption scales linearly with the area of the peak from the high-temperature (630 K) desorption of methanol, as shown in Figure 3b. Note, as discussed earlier, the mass signal of $m/z = 34$ is used for analysis of Figure 3 because it can be safely attributed to only the fragmentation from methanol. This observation can be explained by considering the elemental mass balance for the methanol-exposed $Fe_3O_4(111)$ surface. Chemisorption of methanol (eq 1) creates an equal surface density of D_{ads} and CD_3O_{ads}. Without any additional loss channel for adsorbed D, all methoxy would recombine with D_{ads} during the temperature ramp to 500 K following recombinative desorption as eq 2. Thus, no peak would be expected at temperatures >500 K, an observation that is contrary to our experimental measurements. However, desorption of D_2O at temperatures below 330 K provides an alternative depletion channel for D_{ads}, thus causing incomplete desorption of CD_3O_{ads} species, which remain undesorbed above 500 K. Instead these unrecombined methoxy species desorb through the disproportionation reaction, shown in eq 6, at 630 K. Note that methoxy species have also been observed to remain at comparatively high temperature (610 K) before further oxidizing to CH_2O at VO_x/CeO_2 surface. From analysis of the relative TPD peak areas, we have calculated that at a coverage corresponding to saturation of the TPD peaks, only ∼0.08 ML of methanol is needed to account for the 630 K desorption channel. Thus, our model requires a ∼0.04 ML surface concentration of these weakly bound O atoms on the as-prepared $Fe_3O_4(111)$ surfaces. Once D_2O_{ads} molecules are formed, they compete with adsorbed methanol molecules, as both bind through OD groups, for the same dissociative and molecular adsorption sites. Under these conditions, the data in Figure 3a are consistent with methanol occupying the highest binding-energy sites and with water being desorbed from lower binding-energy sites. The fact that water molecules desorb before methanol molecules (peak temperature vs rising temperature) could be attributed to the stronger intermolecular interactions between methanol and methoxy species as compared to the interaction between water molecules and methoxy species. The above hypothesis is consistent with earlier studies of water interaction with $Fe_3O_4(111)$, which show the presence of a wide range of both dissociative and molecular adsorption sites on $Fe_3O_4(111)$ that lead to thermal desorption in the 200−350 K temperature range.[29]

Scanning Tunneling Microscopy Experiments. To examine the site- and surface-termination dependence of this methanol/iron−oxide reactive system, a series of room-temperature STM imaging experiments were undertaken.

DOI: 10.1021/jp510821g
J. Phys. Chem. C 2015, 119, 1113−1120

These studies benefited from the many reconstructions that are realizable on a magnetite surface. This (111) surface of Fe_3O_4 is a Tasker's type III polar surface[30−32] with apparent surface charge and an infinite dipole moment for the stoichiometric unreconstructed surface. Thus, the $Fe_3O_4(111)$ surface is stabilized via the introduction of defects, reconstruction, and adsorbates. Such a surface, upon preparation in UHV, exhibits several different phases with different terminations: a $Fe_3O_4(111)$ phase with Fe-termination; a FeO(111) phase with O-termination; and a biphase with mixed Fe/O terminations.

The STM images in Figure 4a,b show two macroscopically separated 50 × 50 nm areas of a $Fe_3O_4(111)$ surface, prepared according to the procedure described in the Experimental and Theoretical Methods. This same surface was used in our TPD experiments. The resulting images of the bare surface demonstrate a variety of surface reconstructions. In particular, areas denoted with (A) show the "bi-phase" reconstruction, which in turn is the ordered array of three different surface terminations.[33,34] The area marked (B) shows islands of a "regular" (2 × 2) Fe-terminated $Fe_3O_4(111)$ surface structure growing on top of a biphase area.[33] This same Fe-terminated phase appears as an almost continuous surface structure in the image areas marked (C). Finally, islands are also identified (see the region marked with a D) in the STM image in Figure 4c of a surface reconstruction with an O-terminated FeO(111) local atomic structure.[35,36] STM area scanning, in addition to the nearly perfect (2 × 2) LEED pattern obtained following our surface preparation, allows us to conclude that the "regular" Fe-terminated $Fe_3O_4(111)$ surface phase (marked with C) was the majority structure on this surface.

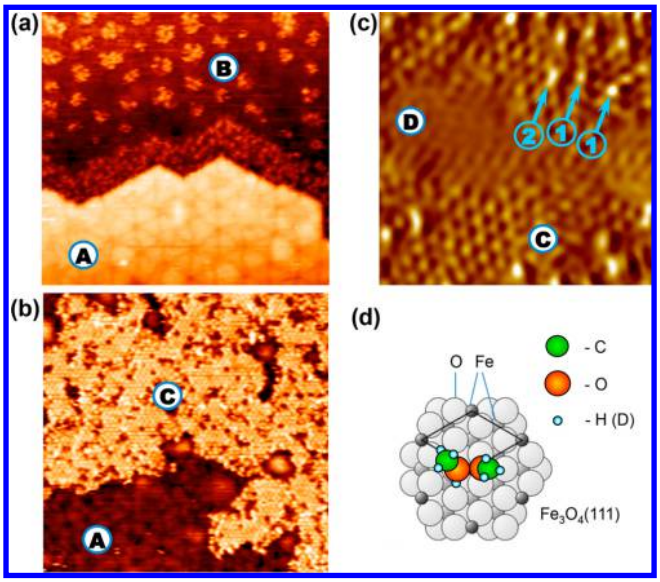

Figure 4. (a and b) 50 × 50 nm^2 room temperature STM images of as-prepared $Fe_3O_4(111)$ surface, acquired at +1.7 V and 10 pA, that show several iron oxide surface reconstructions. "A" in the images denotes the biphase domains, "B" denotes a biphase area with islands of Fe-termination, and "C" denotes an almost continuous (2 × 2) Fe-terminated $Fe_3O_4(111)$ surface. (c) Room temperature STM image (10 × 10 nm^2) acquired at +1.7 V and 1.0 nA, of a $Fe_3O_4(111)$ surface exposed to 0.15 ML of methanol. The image shows that methanol species, three of which are indicated by the blue arrows, are only observed on Fe-terminated $Fe_3O_4(111)$ areas. Note that the O-terminated FeO(111) domains, marked by "D", do not have any methanol species. (d) Schematic of adsorption geometry of chemisorbed methoxy (the right molecule) and molecular methanol (left) on a Fe^{III} site for a (2 × 2) Fe-terminated $Fe_3O_4(111)$ surface, as discussed in the text.

To identify the adsorption sites of methanol on $Fe_3O_4(111)$, we have obtained STM images of the surface after a 0.15 ML dose of deuterated methanol at room temperature. Figure 4c shows a typical constant-height STM image of an iron−oxide surface with adsorbed methanol species. This topograph indicates that the Fe-terminated $Fe_3O_4(111)$ phase, with the characteristic 0.6 × 0.6 nm unit cell over a majority of the surface area, exhibits bright features that appear only after dosing the iron−oxide surface with CD_3OD. On the other hand, the area marked (D) does not have any bright features. These areas are O-terminated FeO(111) domains, and, in agreement with the rationale given in the previous paragraph, we did not see any methanol species on such areas at room temperature, a conjecture supported by the absence of adsorbed species in the figure. In contrast, however, we observe bright features on Fe-terminated $Fe_3O_4(111)$ and interpret these features as adsorbed methanol species; examples are marked with arrows in Figure 4c. In addition, we observe two distinctly different adsorption geometries. One exhibits atop-on-Fe^{III}-ion adsorption geometry, denoted (1) in the figure. Our DFT calculations suggest that dissociative adsorption, with methoxy remaining on the atop Fe sites, is the most stable adsorption configuration. In fact, note that previously water has been observed to dissociate on this surface with OH attached to the Fe sites.[4,20] Thus, the features found atop the Fe^{III}-ion are attributed to methoxy species formed by the deprotonation reaction in eq 1. Note also that dissociated D atoms are likely mobile and not observable at room temperature, as has been inferred above from the temperature of recombinative methanol desorption. In addition, the elongated features, one of which is marked (2) in Figure 4c, are harder to assign to a specific molecular arrangement on the basis of STM images. Possible assignments include two methoxy species occupying neighboring Fe sites or a more complex, perhaps surface-defect-related, feature.

The complex surface structure revealed by STM imaging further enables us to interpret the subtle details observed in the TPD experiments. Note that one possible explanation for the two different molecular adsorption states of methanol, as manifested in the 255 and 290 K TPD desorption peaks, is that these two states originate from different surface phases. As shown in Figure 4a, besides the dominant domain of Fe-terminated $Fe_3O_4(111)$, the "bi-phase" structure also contains domains with Fe-terminated areas, which may be responsible for the relatively small molecular desorption peak (<0.1 ML) observed at 255 K in the TPD experiments. Also, the STM images suggest the presence of a wide variety of defect sites, such as Fe-vacancies or phase boundaries, as the source of weakly bound O atoms, necessary for D_2O desorption in the range 220−340 K. Finally, note that the trace methanol desorption peak (≲0.03 ML) coincides with the multilayer peak at 180 K; this small desorption peak appears well before the completion of a single layer (see Figure 1). Because neither the small peak area (≲0.03 ML) nor its coexistence with submonolayer peaks are expected for second layer or multilayer desorption, this peak is attributed to adsorption on a spatially separated O-terminated region of the surface. In particular, in the absence of exposed Fe ions on such areas, the binding of methanol molecules to surface O atoms can be expected to be

DOI: 10.1021/jp510821g
J. Phys. Chem. C 2015, 119, 1113−1120

driven by hydrogen bonds, as occurs in the binding of methanol to itself in solid form; hence, the overlap of desorption peaks occurs from these areas at 180 K and from multilayers at 165 K.

Finally recall that the recombination reaction (eq 2) would be the rate-limiting step of the desorption process to account for the observed second-order desorption process. This reasoning implies that at least one of the species CD_3O_{ads} or D_{ads} is mobile on the surface at the temperature of the onset of desorption, ~250 K. Because $Fe_3O_4(111)$-adsorbed CD_3O_{ads} species are expected to be bound to Fe^{III} sites, which are twice as far apart as compared to the spacing of the O sites to which D_{ads} are bound, we conclude that D atoms are the mobile moieties on $Fe_3O_4(111)$ at 250 K.

DFT Calculations. Density functional theory simulations were employed to calculate the adsorption energy of methanol on the Fe-terminated $Fe_3O_4(111)$ surface. The results of the calculations are presented schematically in Figure 5. In the

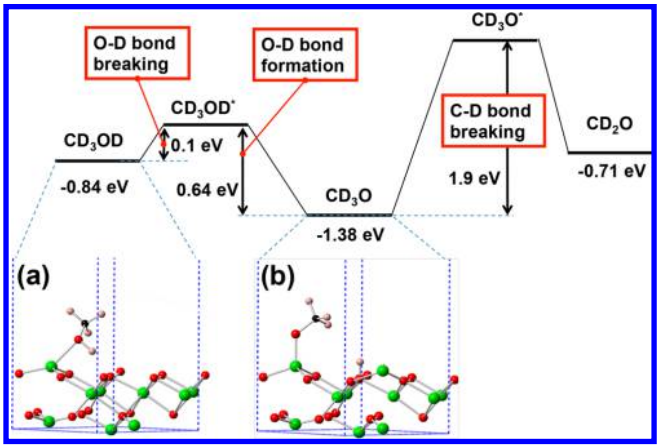

Figure 5. Schematic representation of the results of DFT calculations for methanol adsorption on a Fe-terminated $Fe_3O_4(111)$ surface. Insets (a) and (b) show the optimized surface bonding configurations of the molecular methanol and the CD_3O_{ads} + D_{ads} complex, respectively (O atoms, red; Fe atoms, green; C atoms, black; H(D) atoms, gray).

calculations, methanol is found to be adsorbed on the $Fe_3O_4(111)$ surface molecularly with an adsorption energy of −0.84 eV via Fe_{surf}−O_{mol} bond formation as shown in Figure 5a. However, the dissociative adsorption process (Fe_{surf}−OCD_3, O_{surf}−D) shown in Figure 5b is calculated to be more favored than molecular adsorption with E_{ads} = −1.38 eV and a dissociation barrier of ~0.10 eV, indicating that methanol molecules will experience dissociation promptly upon adsorption onto surface terminating Fe^{III} sites, as shown in eq 1.

If we use the calculated potential barrier of 0.64 eV for the recombination reaction in a straightforward Redhead analysis, we find that the predicted desorption maximum at saturation is ~240 K, a value that is contradictory to our observed peak value of 330 K. However, in an earlier study of water interaction with $Fe_3O_4(111)$, it was shown that for water recombinative desorption the prefactor was about 6 orders of magnitude lower than normally assumed in the Redhead analysis due to a sterically demanding transition state.[29] Because recombinative desorption of methanol and that of water have identical mechanisms, a similarly low pre-exponential factor for methanol desorption may exist and thus may explain the observed discrepancy in the peak temperature for desorption. In addition, note that there is a commonly accepted ~0.1 eV error for DFT calculations; this error could be another contributing factor to the observed discrepancy. Our calculations suggest that at low exposures methanol will undergo deprotonation upon adsorption on a Fe-terminated $Fe_3O_4(111)$ surface, and the resultant methoxy species will assume atop bonding on Fe^{III} ions.

Prior studies on metal oxides, for example, TiO_2, have shown that surface metal ions are the expected absorption sites for both chemisorbed and molecular absorption states. First, the terminating Fe ions are under-coordinated as compared to their full coordination configuration (3 coordinated vs 6 coordinated). Thus, they are strong Lewis acid sites, capable of receiving more than one Lewis base. Second, the low density of Fe^{III} surface sites (even if filled) leaves available surface area for physisorption of intact CD_3OD after chemisorption occurs on each Fe^{III} site, so as to form attached methoxy. Thus, the steric repulsion between methoxy and intact methanol molecules should be minimal and can be compensated for by their strong interaction with Fe ions and also possible hydrogen bonds between intact methanol molecules with the surrounding molecules. Therefore, it is proposed that molecular methanol forms complexes with iron ions of the CD_3O−Fe^{III}−CD_3OD type, as shown schematically in Figure 4d. Note that the presence of the adsorbed methoxy group would be expected to weaken the Lewis acidity of the Fe^{III} sites, thus causing the second adsorbed molecule not to deprotonate.

The above tentative model would predict a 1:1 ratio between the molecularly and dissociatively adsorbed methanol molecules at full monolayer coverage. To confirm this model, we determined the intensity of the total integrated TPD peaks in Figure 1. In doing these calculations, we took into the account the fact that dissociatively adsorbed methanol is responsible for both the 330−360 and the 630 K desorption features. This prediction is confirmed within our experimental uncertainty by our measured ratio of 1.1:0.9. Finally, note that the binding energy of 0.69−0.79 eV, derived from the positions of our molecular desorption TPD peaks, is lower than the 0.84 eV value calculated for an isolated methanol molecule (see Figure 5). This decrease in binding energy is reasonable because the presence of an additional methoxy moiety on the same Fe^{III} site will be expected to decrease the molecular binding energy as a result of steric hindrance in accord with our model of the absorption process.

Finally, we consider the reactions observed at the highest temperatures used here, that is, the disproportionation reaction. During methanol deposition, the chemisorption process expressed in eq 1 leaves an equal number of methoxy and D_{ads} species on the surface. If both species remain intact on the surface up to the temperature that allows the reverse process (eq 2) to occur, all methoxy groups would desorb as methanol through recombinative desorption at ~360 K. However, in our experiments, we detected desorption of D_2O below 320 K that depletes the D_{ads} population. For this reason, some methoxy species are not able to desorb through recombination due to the lack of D_{ads}; such methoxy groups survive to the temperature at which further decomposition routes become activated. The dissociation barrier of methoxy (CD_3O) to formaldehyde (CD_2O) through C−H bond scission is calculated to be ~1.9 eV according to DFT simulations, as shown in Figure 5. On the other hand, Redhead analysis suggests that the activation barrier for a 630 K desorption peak is ~1.75 eV, thus providing support of our proposed mechanism, which is summarized by eqs 3−5. In addition, as

DOI: 10.1021/jp510821g
J. Phys. Chem. C 2015, 119, 1113−1120

mentioned above, the binding energy of an adsorbed formaldehyde molecule was calculated to be 0.71 eV, thus confirming the immediate desorption after formation at 630 K, as observed in our TPD experiments.

SUMMARY

Our experiments show that methanol adsorbs through deprotonation on a $Fe_3O_4(111)$ surface up to ~0.5 ML; it then adsorbs to the surface nondissociatively for higher coverages up to 1 ML. The methanol deprotonation leaves methoxy CD_3O_{ads} and hydrogen D_{ads} species on the surface. Any excess molecular methanol will desorb from a temperature-ramped surface at temperatures below 300 K, while the methoxy species are stable up to room temperature. Surface methoxy species also recombine with D_{ads} species and desorb as methanol in the 330−360 K temperature range. STM imaging has clarified the nature of the adsorbed species. For example, atomic scale imaging shows that only Fe-terminated areas chemisorb methanol, while O-terminated FeO(111) domains remain methanol free at room temperature. STM images also show that methoxy binds to the surface via the atop site of surface Fe^{III} ions.

Chemical transformation of methanol was only observed via formation of formaldehyde as a result of a disproportionation reaction between two adsorbed methoxy species at ~630 K, as shown in eq 6. We attribute the continued adsorption of methoxy groups on the surface at this relatively high temperature to the fact that some D_{ads} species react with surface oxygen atoms O_{surf} and desorb as D_2O below 320 K. Because of the partial removal of D_{ads} species, only a limited amount of methoxy radicals recombinatively desorb at 330−360 K, and the remainder stays on the surface to higher temperatures. Thus, the overall reaction can be written as

$$CD_3OD_{gas} + O_{surf} \rightarrow D_2O_{gas} + CD_2O_{gas} \quad (7)$$

The extent of this reaction is limited by the surface concentration of weakly bound O_{surf} species, estimated to be ~0.04 ML. These species are apparently replenished each time the sample is heated to 1000 K. We cannot identify the specific nature of these oxygen atoms, but the wide variety of $Fe_3O_4(111)$ surface reconstructions seen in STM images suggests that these O_{surf} species could be related to surface defects such as those found at phase boundaries.

At the atomic level, formation of formaldehyde proceeds through C−D bond scission (see eq 3). Yet, no further thermal decomposition of formaldehyde via C−D bond scission was observed in the current experiments. Also, no hydrocarbon C_xH_y species were found in the desorption products, although it is known that a competing reaction channel exists involving the scission of a C−O bond resulting in hydrocarbon species.[10] We thus summarize the observed catalytic chemistry of methanol on a $Fe_3O_4(111)$ surface as partial oxidation to formaldehyde (shown in eq 7). Similar chemistry has been demonstrated on a CeO_2-supported vanadium oxide surface.[28]

AUTHOR INFORMATION

Corresponding Author

*E-mail: osgood@columbia.edu.

Notes

The authors declare no competing financial interest.

ACKNOWLEDGMENTS

We are indebted to Professor Jonathan Owen for stimulating discussions about iron−oxide chemistry and surface structure. This work was funded by the U.S. Department of Energy under Grant nos. DE-FG02-90ER14104 (R.M.O.), DE-FG02-05ER15730 (M.F.-S. and G.W.F.), DE-FG02-88ER13937 (G.W.F), and EFRC Award DE-SC0001085 (G.W.F.). We acknowledge financial support from the New York State Office of Science, Technology, and Academic Research (NYSTAR). Equipment and material support was provided by the National Science Foundation under grants CHE-07-01483, CHE-10-12058 (G.W.F.), and DMR-1206768 (R.M.O.). Work at Los Alamos National Laboratory (E.R.B., X.-D.W.) was supported by LDRD program at LANL. Some of the calculations were performed on the Chinook and Cascade computing systems at the Environmental Molecular Sciences Laboratory (EMSL) at PNNL. The Los Alamos National Laboratory is operated by Los Alamos National Security, LLC, for the National Nuclear Security Administration of the U.S. Department of Energy under contract DE-AC5206NA25396.

REFERENCES

(1) Hacker, V.; Fankhauser, R.; Faleschini, G.; Fuchs, H.; Friedrich, K.; Muhr, M.; Kordesch, K. Hydrogen Production by Steam−Iron Process. *J. Power Sources* **2000**, *86*, 531−535.

(2) Rim, K. T.; Fitts, J. P.; Müller, T.; Adib, K.; Camillone, N., III; Osgood, R. M.; Joyce, S. A.; Flynn, G. W. CCl_4 Chemistry on the Reduced Selvedge of a α-$Fe_2O_3(0001)$ Surface: A Scanning Tunneling Microscopy Study. *Surf. Sci.* **2003**, *541*, 59−75.

(3) Guo, Q.; McBreen, P. H.; Möller, P. J. CH_3OH Adsorption on Clean and Cu-Predeposited α-$Fe_2O_3(0001)$ Surfaces. *Surf. Sci.* **1999**, *423*, 19−23.

(4) Joseph, Y.; Kuhrs, C.; Ranke, W.; Ritter, M.; Weiss, W. Adsorption of Water on FeO(111) and $Fe_3O_4(111)$: Identification of Active Sites for Dissociation. *Chem. Phys. Lett.* **1999**, *314*, 195−202.

(5) Adib, K.; Totir, G. G.; Fitts, J. P.; Rim, K. T.; Mueller, T.; Flynn, G. W.; Joyce, S. A.; Osgood, R. M. Chemistry of CCl_4 on $Fe_3O_4(111)$-(2 × 2) Surfaces in the Presence of Adsorbed D_2O Studied by Temperature Programmed Desorption. *Surf. Sci.* **2003**, *537*, 191−204.

(6) Carlos-Cuellar, S.; Li, P.; Christensen, A. P.; Krueger, B. J.; Burrichter, C.; Grassian, V. H. Heterogeneous Uptake Kinetics of Volatile Organic Compounds on Oxide Surfaces Using a Knudsen Cell Reactor: Adsorption of Acetic Acid, Formaldehyde, and Methanol on α-Fe_2O_3, α -Al_2O_3, and SiO_2. *J. Phys. Chem. A* **2003**, *107*, 4250−4261.

(7) Leist, U.; Ranke, W.; Al-Shamery, K. Water Adsorption and Growth of Ice on Epitaxial $Fe_3O_4(111)$, FeO(111) and Fe_2O_3(Biphase). *Phys. Chem. Chem. Phys.* **2003**, *5*, 2435−2441.

(8) Camillone Iii, N.; Adib, K.; Fitts, J. P.; Rim, K. T.; Flynn, G. W.; Joyce, S.; Osgood, R. M. Surface Termination Dependence of the Reactivity of Single Crystal Hematite with CCl_4. *Surf. Sci.* **2002**, *511*, 267−282.

(9) Rim, K. T.; Müller, T.; Fitts, J. P.; Adib, K.; Camillone, N., III; Osgood, R. M.; Joyce, S. A.; Flynn, G. W. Scanning Tunneling Microscopy and Theoretical Study of Competitive Reactions in the Dissociative Chemisorption of CCl_4 on Iron Oxide Surfaces. *J. Phys. Chem. B* **2004**, *108*, 16753−16760.

(10) Bäumer, M.; Libuda, J.; Neyman, K. M.; Rösch, N.; Rupprechter, G.; Freund, H.-J. Adsorption and Reaction of Methanol on Supported Palladium Catalysts: Microscopic-Level Studies from Ultrahigh Vacuum to Ambient Pressure. *Phys. Chem. Chem. Phys.* **2007**, *9*, 3541−3558.

(11) Cacciola, G.; Antonucci, V.; Freni, S. Technology up Date and New Strategies on Fuel Cells. *J. Power Sources* **2001**, *100*, 67−79.

(12) King, J. M.; O'Day, M. J. Applying Fuel Cell Experience to Sustainable Power Products. *J. Power Sources* **2000**, *86*, 16−22.

DOI: 10.1021/jp510821g
J. Phys. Chem. C 2015, 119, 1113−1120

(13) Ramirez, D.; Beites, L. F.; Blazquez, F.; Ballesteros, J. C. Distributed Generation System with Pem Fuel Cell for Electrical Power Quality Improvement. *Int. J. Hydrogen Energy* **2008**, *33*, 4433−4443.
(14) Boucher, M. B.; Yi, N.; Gittleson, F.; Zugic, B.; Saltsburg, H.; Flytzani-Stephanopoulos, M. Hydrogen Production from Methanol over Gold Supported on Zno and CeO_2 Nanoshapes. *J. Phys. Chem. C* **2011**, *115*, 1261−1268.
(15) Sá, S.; Silva, H.; Brandão, L.; Sousa, J. M.; Mendes, A. Catalysts for Methanol Steam Reforming−a Review. *Appl. Catal., B* **2010**, *99*, 43−57.
(16) Palo, D. R.; Dagle, R. A.; Holladay, J. D. Methanol Steam Reforming for Hydrogen Production. *Chem. Rev.* **2007**, *107*, 3992−4021.
(17) Yongtaek, C.; Stenger, H. G. Fuel Cell Grade Hydrogen from Methanol on a Commercial $Cu/Zno/Al_2O_3$ Catalyst. *Appl. Catal., B* **2002**, *38*, 259−269.
(18) Camillone, N., III; Adib, K.; Fitts, J. P.; Rim, K. T.; Flynn, G. W.; Joyce, S. A.; Osgood, R. M. Surface Termination Dependence of the Reactivity of Single Crystal Hematite with CCl_4. *Surf. Sci.* **2002**, *511*, 267−282.
(19) Rim, K. T.; Eom, D.; Liu, L.; Stolyarova, E.; Raitano, J. M.; Chan, S.-W.; Flytzani-Stephanopoulos, M.; Flynn, G. W. Charging and Chemical Reactivity of Gold Nanoparticles and Adatoms on the (111) Surface of Single-Crystal Magnetite: A Scanning Tunneling Microscopy/Spectroscopy Study. *J. Phys. Chem. C* **2009**, *113*, 10198−10205.
(20) Rim, K. T.; Eom, D.; Chan, S.-W.; Flytzani-Stephanopoulos, M.; Flynn, G. W.; Wen, X.-D.; Batista, E. R. Scanning Tunneling Microscopy and Theoretical Study of Water Adsorption on Fe_3O_4: Implications for Catalysis. *J. Am. Chem. Soc.* **2012**, *134*, 18979−18985.
(21) Kresse, G.; Hafner, J. Ab Initio Molecular Dynamics for Liquid Metals. *Phys. Rev. B* **1993**, *47*, 558−561.
(22) Blöchl, P. E. Projector Augmented-Wave Method. *Phys. Rev. B* **1994**, *50*, 17953−17979.
(23) Kresse, G.; Joubert, D. From Ultrasoft Pseudopotentials to the Projector Augmented-Wave Method. *Phys. Rev. B* **1999**, *59*, 1758−1775.
(24) Dudarev, S. L.; Botton, G. A.; Savrasov, S. Y.; Humphreys, C. J.; Sutton, A. P. Electron-Energy-Loss Spectra and the Structural Stability of Nickel Oxide:An Lsda+U Study. *Phys. Rev. B* **1998**, *57*, 1505.
(25) Henderson, M. A.; Otero-Tapia, S.; Castro, M. E. The Chemistry of Methanol on the TiO_2(110) Surface: The Influence of Vacancies and Coadsorbed Species. *Faraday Discuss.* **1999**, *114*, 313−329.
(26) Wu, M. C.; Estrada, C. A.; Corneille, J. S.; Goodman, D. W. Model Surface Studies of Metal Oxides: Adsorption of Water and Methanol on Ultrathin MgO Films on Mo(100). *J. Chem. Phys.* **1992**, *96*, 3892−3900.
(27) NIST Mass Spec Data Center. In *Mass Spectra in NIST Chemistry WebBook, NIST Standard Reference Database Number 69*; Linstrom, P. J., Mallard, W. G., Eds.; National Institute of Standards and Technology: Gaithersburg, MD, retrieved October 16, 2014; http://webbook.nist.gov.
(28) Feng, T.; Vohs, J. A TPD Study of the Partial Oxidation of Methanol to Formaldehyde on CeO_2-Supported Vanadium Oxide. *J. Catal.* **2004**, *221*, 619−629.
(29) Joseph, Y.; Ranke, W.; Weiss, W. Water on FeO(111) and Fe_3O_4(111): Adsorption Behavior on Different Surface Terminations. *J. Phys. Chem. B* **2000**, *104*, 3224−3236.
(30) Tasker, P. W. The Stability of Ionic Crystal Surfaces. *J. Phys. C: Solid State Phys.* **1979**, *12*, 4077−4984.
(31) Noguera, C. *Physics and Chemistry at Oxide Surfaces*; Cambridge University Press: UK, 1996.
(32) Noguera, C. Polar Oxide Surfaces. *J. Phys.: Condens. Matter* **2000**, *12*, R367−R410.
(33) Shaikhutdinov, S. K.; Ritter, M.; Wang, X. G.; Over, H.; Weiss, W. Defect Structures on Epitaxial Fe_3O_4(111) Films. *Phys. Rev. B* **1999**, *60*, 11062−11069.
(34) Condon, N. G.; Leibsle, F. M.; Parker, T.; Lennie, A. R.; Vaughan, D. J.; Thornton, G. Biphase Ordering on Fe_3O_4(111). *Phys. Rev. B* **1997**, *55*, 15885−15894.
(35) Galloway, H.; Sautet, P.; Salmeron, M. Structure and Contrast in Scanning Tunneling Microscopy of Oxides: FeO Monolayer on Pt (111). *Phys. Rev. B* **1996**, *54*, R11145.
(36) Rim, K. T.; Eom, D.; Chan, S.-W.; Flytzani-Stephanopoulos, M.; Flynn, G. W.; Wen, X.-D.; Batista, E. R. Scanning Tunneling Microscopy and Theoretical Study of Water Adsorption on Fe_3O_4: Implications for Catalysis. *J. Am. Chem. Soc.* **2012**, *134*, 18979−18985.

DOI: 10.1021/jp510821g
J. Phys. Chem. C 2015, 119, 1113−1120